AIAA JOURNAL
Vol. 41, No. 7, July 2003

Hydroxyl Formation Mechanisms and Models in High-Altitude Hypersonic Flows

N. E. Gimelshein* and D. A. Levin†
Pennsylvania State University, University Park, Pennsylvania 16802
and
S. F. Gimelshein‡
George Washington University, Washington, D.C. 20052

The formation of vibrationally hot OH is examined for a rarefied flow about a sphere at 80 and 100 km using the direct simulation Monte Carlo method. Four main processes are considered leading to OH production in the flow, which include water dissociation, exchange reaction between water and atomic oxygen, and exchange reactions between hydrogen (H and H_2) and oxygen (O_2 and O). The principal mechanism of OH production at 100 km is shown to be the $H + O_2 \rightarrow OH + O$ reaction, with the maximum OH temperature greater than 5000 K. Water dissociation is found to be the most important source of OH at 80 km, with the maximum vibrational temperature of approximately 2500 K. The molecular dynamics results incorporated into the direct simulation Monte Carlo method are used to simulate water dissociation by N_2 and are compared to the results obtained by the conventional total collision energy model. The OH spatial distribution along the stagnation line predicted by the molecular dynamics approach is significantly different than that obtained with the total collisional energy model.

I. Introduction

THE modeling of ultraviolet emissions from hypersonic bow shocks provides an indication of the flowfield gas properties and compliments the usual hypersonic flight surface diagnostics of temperature and pressure. Moreover, the prediction of ultraviolet radiation from hypersonic vehicles is an important engineering application relevant to the prediction of passive optical signatures. Despite the strong operational and scientific reasons for measuring optical emissions from hypersonic vehicles, such data are rare. Spectral radiation from high-energy rarefied flows provides a sensitive metric for the evaluation of energy exchange and chemical reaction models. The bow shock ultraviolet flight experiments[1] (BSUV) obtained spectra of OH($A^2\Sigma^+ - X^2\Pi$) UV radiation between altitudes of 100 and 80 km. These experiments indicate that the OH(A) species formed in rarefied, high-energy flows have internal energies much greater than that of the bulk flow. Because there are so few collisions in these flows, the spectral data may be used to test the ability of theory to model near-nascent distributions of chemically produced radiating species and energy exchange. The UV spectra of OH(A) are well defined and originate from a single excited electronic state. Under rarefied conditions, the OH(A) UV spectra are sensitive to the chemical processes involved in OH formation.

UV radiation from the OH (A) system has been studied extensively in the combustion and atmospheric sciences communities.[2] Earlier work[3] demonstrated the sensitivity of the OH spectra to variation in the vibrational temperature. It was shown that the ratio of the peak heights at 2800 Å (due to the 1–0 transition) and 3100 Å (due to the 0–0 transition) depends mainly on the vibrational temperature.[3] An OH vibrational temperature in the range of 4000–7000 K was derived from the spectral data, demonstrating that the OH vibrational temperature is significantly higher than the predicted shock-layer bulk (N_2) vibrational temperature of ~700 K.

More detailed treatment of the coupling of the flow and radiation modeling has been undertaken for the OH(A) system.[4] This work, however, did not lead to OH vibrational temperatures consistent with the BSUV 2. In earlier work,[5] we performed a detailed modeling of vibrational temperatures and distributions of OH produced by collision-induced water dissociation using unimolecular dynamics results incorporated into the direct simulation Monte Carlo (DSMC) method.[6] A comparison was performed between the total collision energy (TCE) model[7] of the DSMC method and the unimolecular dynamics approach parametrizing the different contributions of the relative translational energy to the energy of water dissociation. It was found that a 10% contribution of translational energy gave results similar to those of TCE, whereas 100% contribution of translational energy gave OH vibrational temperatures significantly higher than predicted by traditional DSMC models.

The goal of this work is to investigate different chemical processes that may lead to vibrationally hot OH in the bow shock at high altitudes and to estimate their effect on the overall vibrational temperature in the flow. The DSMC method is used to model the external flow over a 0.2-m-diam sphere at altitudes of 80 and 100 km, two freestream conditions of the BSUV 2 experiment. An overview of the potentially important reaction processes is given in the next section. The model uncertainties associated with the OH production reactions are then presented along with the details of modeling the postcollisional energy partitioning. An alternative to the conventional TCE model for water dissociation, based on the quasi-classical treatment of the water dissociation by molecular nitrogen, is presented. The main idea of using molecular dynamics (MD) cross sections in the DSMC is to assess the influence of strong nonequilibrium between internal and translational modes on the reaction process as compared to the conventional DSMC models, such as TCE. Finally, the results of the computations that elucidate the contribution of different reactions to the production of vibrationally hot OH are discussed.

II. Modeling of OH Production Mechanisms

Previous work considered the OH production as a result of water dissociation using an approximate model based on unimolecular dynamics and the TCE model.[5] In this work, we extend the unimolecular dynamics dissociation of water to a full scattering calculation, as

Received 5 February 2002; revision received 15 July 2002; accepted for publication 1 September 2002.

*Graduate Student, Department of Aerospace Engineering, 135 Hammond Building.
†Associate Professor, Department of Aerospace Engineering, 233 Hammond Building. Senior Member AIAA.
‡Senior Research Scientist, Department of Chemistry; currently Senior Research Associate, Department of Aerospace Engineering, Pennsylvania State University, 230 Hammond Building, University Park, PA 16802.

Table 1 Freestream conditions

Condition	80 km	100 km
Total number density, m^{-3}	4.18×10^{20}	1.19×10^{19}
Temperature, K	185	181
O_2 mole fraction	0.21	0.18
N_2 mole fraction	0.79	0.78
H_2O mole fraction	5.6×10^{-6}	7.2×10^{-7}
OH mole fraction	4.3×10^{-9}	2.0×10^{-10}
O mole fraction	——	0.04
H mole fraction	5.0×10^{-8}	5×10^{-6}
H_2 mole fraction	5.3×10^{-7}	2.4×10^{-7}

Table 2 Rate coefficients (m^3s^{-1}) for OH production reactions

	$k = AT^n \exp(-E/kT)$			
Reaction	A	n	E/k_B, K	Reference
$H_2O + N_2 \rightarrow OH + H + N_2$	5.81×10^{-15}	0.000	−53,000.0	2
$H_2O + O_2 \rightarrow OH + H + O_2$	1.13×10^{-7}	−1.31	−59,400.0	2
$H_2O + O \rightarrow OH + H + O$	1.13×10^{-7}	−1.31	−59,400.0	2
$O + H_2O \rightarrow OH + OH$	1.13×10^{-16}	0.00	−9,240.0	2
$H + O_2 \rightarrow OH + O$	1.66×10^{-16}	0.00	−7,690.0	8
$H_2 + O \rightarrow OH + H$	3.12×10^{-16}	0.00	−6,897.5	26

well as consider other mechanisms that may potentially impact both the OH production and vibrational energy distribution. We investigate the relative importance of different OH production reactions at altitudes between 80 and 100 km, which will depend on the number densities of the chemical species and the reaction cross sections. Freestream concentrations of reactants and reaction rate constants are given in Tables 1 and 2, respectively.

There are four reaction mechanisms that may significantly contribute to the total OH production and, therefore, OH vibrational populations:

$$H_2O + M \rightarrow OH + H + M \quad (1)$$

$$H_2O + O \rightarrow OH + OH \quad (2)$$

$$O_2 + H \rightarrow OH + O \quad (3)$$

$$H_2 + O \rightarrow OH + H \quad (4)$$

where $M = N_2, O_2$, and O. Process (1) represents water dissociation, and processes (2–4) describe the formation of OH by exchange reactions.

The water-dissociation mechanism [Eq. (1)] was studied in a previous paper,[5] where we compared reaction models based on unimolecular dynamics with TCE in DSMC simulations. In Ref. 5 we presented calculations of vibrational distributions of OH formed by water unimolecular dissociation with parameterized collisional energy transfer before dissociation calculations. The post-water-dissociative nascent OH vibrational and rotational state distributions were calculated from the semiclassical molecular dynamics trajectory method. Although not a complete treatment of the water-dissociation process, the previous work[5] suggested that the dissociation process produces mostly vibrationally cold OH products due to a high heat of reaction for the dissociation of water. Moreover, the relatively slow relaxation of the water vibrational modes, as compared to its translational and rotational modes, results in strong vibrational–translational nonequilibrium even though the flow translational temperature is as high as 15,000 K at 80 km (Knudsen number of ~0.01).

The comparison of water-dissociation rates as a function of temperature is given in Fig. 1 for three collision partners, N_2, O_2, and O. The rates for the last two partners are expected to be similar. Because N_2 outnumbers O_2 by a factor of four, we can expect the contribution from those two colliders to be close. However, the reaction rates are known for those reactions only for temperatures up to 2000 or 3000 K. The data for higher temperatures are mostly their extrapolation and incorporation of various theoretical predictions.

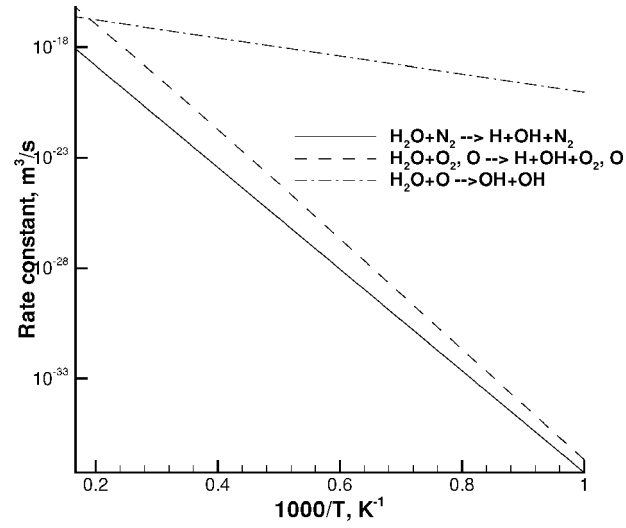

Fig. 1 Comparison of reaction rates for water dissociation and exchange reactions.

Moreover, the temperature-dependent rates cannot be used directly in DSMC simulations. The application of the DSMC method requires the knowledge of energy-dependent cross sections. In previous work,[5] we have used the trajectory calculation data for the unimolecular water dissociation to model the probabilities of water-dissociation reactions. The key assumption of that model is that the interaction time is the ratio of the effective variable hard-sphere diameter of water and the collider (N_2) to their relative velocity. The validity of this assumption is questionable, and detailed trajectory calculations on an H_2O–N_2 potential energy surface are carried out in this work aimed at obtaining the state-dependent reaction cross sections for water dissociation.

The cross sections for the water exchange reaction and water dissociation by O and O_2 are not available at present. [The interaction of H_2O and O is being studied, but reaction cross sections have not been published (private communication with D. R. Yarkoni).] To compare relative contributions from all of the reactions, we need to model them consistently. To this end, the conventional total collision energy (TCE) model based on the collision theory for chemical reactions will be used for the computations in Sec. V.

The formation of OH by Eq. (2) is qualitatively different from dissociation, with a smaller reaction threshold and weaker dependence of OH internal energy on the internal energy of water. Whereas any air species may dissociate water, only atomic oxygen can participate in the exchange reaction. As Table 1 shows, there is no atomic oxygen in the freestream at 80 km; hence, the principal O source is the oxygen-dissociation reactions in the shock front. The concentration of atomic oxygen at 100 km, however, is about 4%, which makes this reaction path comparable to dissociation in terms of OH production. The comparison between the dissociation and exchange reaction rates are given in Fig. 1. Note that the rates are shown for a temperature T and thermal equilibrium is assumed between translational and internal modes. Significant thermal nonequilibrium in the shock requires one to use a full flow model to predict the relative importance of these reactions.

The hydroxyl radical may also be formed by reaction of $O_2 + H$ [Eq. (3)]. There are several recent measurements of rates and cross sections for this reaction, for example, Ref. 8. However, to estimate its contribution into OH production, it is also necessary to have good estimates of the concentrations of the reactants. Whereas the concentration of O_2 is well known at both altitudes of interest, there are few measurements of H concentration. At altitudes below 100 km, H concentration is subject to diurnal variation. In our calculations we used freestream H concentration values from Ref. 9 (also private communication with R. Bevelacqua). In contrast to the variable concentration of the major species due to longitudinal and seasonal variations of 50%, the uncertainty in minor species concentrations of H and H_2 is an order of magnitude.[9] The vibrational temperature of

OH produced by this reaction could be even higher than that of OH, produced by $H_2O + O$ exchange due to a lower reaction heat and fewer number of modes between which the energy of the colliding partners is distributed.

Finally, OH may be formed by H_2 reacting with O [Eq. (4)]. This reaction can in principle produce OH with even higher vibrational temperature than the preceding one because of its low reaction heat. However, it is difficult to estimate its contribution to OH production because little is known about the concentration of H_2. As mentioned earlier, at 80 km the only source of atomic oxygen is the molecular oxygen dissociation in the shock front, so that atomic oxygen concentration is probably too low for this reaction to have a significant impact on OH production. Diurnal variation of H_2 is expected to be small at the altitudes of interest. At 100 km, H_2 concentration is expected to be about 5×10^{12} molecule/m^3, and this reaction may have some impact on the overall OH production and temperature.

A major part of the chemistry modeling involves the issue of how to partition the postcollisional energy among the reaction products. Because there are two types of reactions studied in this work (dissociation and exchange), different energy redistribution models were used for these reaction types. For dissociation, the Haas model[10] was used. The algorithm of the model is as follows. First, the total collision energy E_c is calculated. Then all energies (relative translational, rotational, and vibrational) are multiplied by a factor of $(E_c - E_d)/E_c$, where E_d is the water-dissociation threshold. The new velocities of H_2O and the collision partner are calculated. Afterward, the water molecule is divided into OH and H. The energies of the OH–H pair (relative translational and OH internal energies) are calculated so that the magnitude is proportional to the number of degrees of freedom of the corresponding modes and that the sum is equal to the sum of rotational and vibrational energies of water. Finally, new velocities of OH and H are calculated using the new relative translational energy of the OH–H pair and the velocity of the center of mass equal to the water velocity. With such a redistribution, the internal energies of OH are proportional to the internal energy of H_2O.

The proportional decrease of mode energies utilized in the Haas model[10] cannot generally be applied for exchange reactions. For these reactions, therefore, the discrete Larsen–Borgnakke model[11] was used. In this model, the energy available after the reaction (total collision energy reduced by reaction heat) is redistributed, assuming local equilibrium in such a way that the average energy going into rotational, vibrational, and translational modes is proportional to the number of degrees of freedom in these modes. The number of vibrational degrees of freedom was calculated based on the local translational temperature using a simple harmonic oscillator approximation.

III. Trajectory Calculation of Water Dissociation Cross Sections

Quasi-classical trajectories (QCT) calculations of the MD method enable one to obtain probabilities, cross sections, and rate constants for fundamental elementary reactions. Because these quantities mostly depend on the motion of atomic nuclei, a classical treatment has been shown to provide a good approximation for the investigation of such reaction mechanisms. To perform QCT calculations, it is necessary to know the potential energy surface (PES), which reflects the change in electronic energy as a function of the internuclear distances. The MD method is known as quasi classical when quantum mechanical calculations are performed to determine the electronic potential surface energy.

To perform trajectory calculations, the following PES was developed. The internal degrees of freedom of N_2 were neglected, and because in the reaction of interest no atom exchange occurs, the potential was written as

$$V = V^{H_2O} + V^{int}$$

where V^{H_2O} is the scattering potential of the water molecule and V^{int} is the interaction potential. The water potential V^{H_2O} was taken from the work of Murrell et al.,[12] who obtained an accurate quantum mechanical solution for the ground state of water using a two-value surface approach. V^{int} was represented as the sum of three two-body terms:

$$V^{int} = V_{O-N_2}(R_{O-N_2}) + V_{H-N_2}(R_{H^1-N_2}) + V_{H-N_2}(R_{H^2-N_2})$$

where R_{O-N_2}, $R_{H^1-N_2}$, and $R_{H^2-N_2}$ are the distances between the respective atoms of the water molecule and the center of mass of the N_2 molecule and

$$V_{O-N_2}(R) = A_1 \times \exp(-a_1 R) + B_1 \exp(-b_1 R) - C_{ON}/R^6$$

$$V_{H-N_2}(R) = A_2 \times \exp(-a_2 R) + B_2 \exp(-b_2 R) - C_{HN}/R^6$$

The form of the two-body potential, taken from Ref. 13, contains a Lennard–Jones[11] attractive term and an exponential repulsive term. The potential energy surface was fitted to a set of ab initio points, calculated using the GAMESS computational quantum chemistry program.[14] The values of the parameters are given in the Table 3.

The initial conditions for the classical trajectories were specified using the microcanonical sampling method.[15] For the calculations, the maximum impact parameter b_{max} has to be specified and should be large enough so that the dissociation cross section is independent of b_{max}. The appropriate value of b_{max} was found to be 2 Å. Figure 2 shows the reaction probability as a function of internal water energy for different relative N_2–H_2O velocities. The reaction probability is the ratio of reaction cross section obtained from the MD calculations reaction normalized by the variable hard sphere (VHS) total collision cross section.[6] The VHS diameter was assumed to be 4 Å, and the exponent was 0.37.

To compare the trajectory calculations with the experimental data, the reaction rate was calculated for several temperatures using cross sections obtained from the MD calculations.

Table 3 Parameters used in potential energy surface

Parameter	Value
A_1	2.357×10^{-15}
a_1, Å^{-1}	4.6727
B_1	1.275×10^{-15}
b_1, Å^{-1}	2.7828
A_2	1.2444×10^{-17}
a_2, Å^{-1}	3.4325
B_2	1.170×10^{-17}
b_2, Å^{-1}	3.4620
C_{ON}, Å^6	3.111×10^6
C_{HN}, Å^6	2.109×10^3

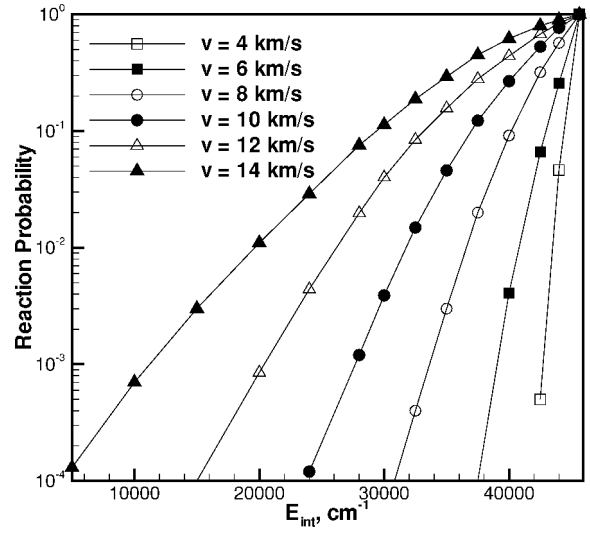

Fig. 2 Probabilities for $H_2O + N_2$ reaction as a function of water internal energy.

The calculation of the reaction rate coefficient required the evaluation of

$$k_d(T) = \sum_{v_1}\sum_{v_2}\sum_{r_1}\sum_{r_2} f(v_1)f(v_2)f(r_1)f(r_2) \times \int_0^\infty \sigma(E_t, E_{\text{int}})gf(E_t)\,\mathrm{d}E_t \tag{5}$$

where T is the temperature; v_1, v_2, r_1, and r_2 denote the summation over all vibrational and rotational modes of the first (water) and the second (nitrogen) molecules; $\sigma(E_t, E_{\text{int}})$ is the calculated reaction cross section; and E_t and g are the relative translational energy and collision velocity of the pair, respectively. The rate coefficient [Eq. (5)] is evaluated using a Monte Carlo approach. A logarithmic interpolation was used to determine the values of the reaction cross section for energies between the calculated E_t^i and E_t^{i+1} and E_{int}^j and E_{int}^{j+1} points,

$$\sigma(E_t, E_{\text{int}}) = \exp\left\{ \frac{E_t^{i+1}-E_t}{E_t^{i+1}-E_t^i}\frac{E_{\text{int}}^{j+1}-E_{\text{int}}}{E_{\text{int}}^{j+1}-E_{\text{int}}^j}\ell n\left[\sigma\left(E_t^i, E_{\text{int}}^j\right)\right] + \frac{E_t^{i+1}-E_t}{E_t^{i+1}-E_t^i}\frac{E_{\text{int}}-E_{\text{int}}^j}{E_{\text{int}}^{j+1}-E_{\text{int}}^j}\ell n\left[\sigma\left(E_t^i, E_{\text{int}}^{j+1}\right)\right] + \frac{E_t-E_t^i}{E_t^{i+1}-E_t^i}\frac{E_{\text{int}}^{j+1}-E_{\text{int}}}{E_{\text{int}}^{j+1}-E_{\text{int}}^j}\ell n\left[\sigma\left(E_t^{i+1}, E_{\text{int}}^j\right)\right] + \frac{E_t-E_t^i}{E_t^{i+1}-E_t^i}\frac{E_{\text{int}}-E_{\text{int}}^j}{E_{\text{int}}^{j+1}-E_{\text{int}}^j}\ell n\left[\sigma\left(E_t^{i+1}, E_{\text{int}}^{j+1}\right)\right]\right\}$$

The functions f in Eq. (5) are the equilibrium distribution functions. The translational function is

$$f(E_t) = \left[E_t^{\xi/2-1}\Big/\Gamma(\xi/2)\right]\exp[-(E_t/kT)]$$

For the rotational and vibrational modes they are written as

$$f(l) = g(l)\exp[-E(l)/kT]/Q$$

where l is either rotational or vibrational level, g is the degeneracy, E is the energy, and

$$Q = \sum_l g(l)\exp\left[-\frac{E(l)}{kT}\right]$$

is the partition function. The expressions for g, E, and Q may be found in Ref. 16.

The rate coefficient was estimated for several temperatures, and the obtained values were compared with the Arrhenius data for this reaction (Table 2). As Fig. 3 shows, there is a reasonable agreement between the Arrhenius rates and the rates obtained from the MD calculations. The agreement seems to be poorer at lower temperatures and is most likely due to the inadequacy of the scattering potential V. Note that the number of trajectories was larger for lower temperatures to provide a constant statistical error of better than 20% in the entire temperature range. The number of trajectories was approximately 100,000 for 3000 K.

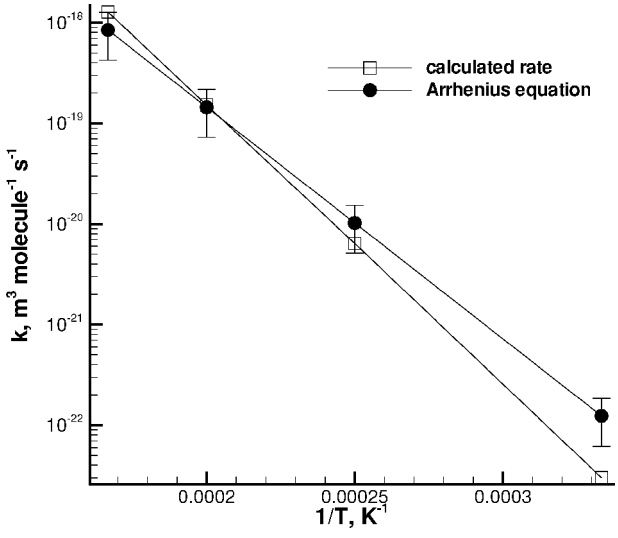

Fig. 3 Comparison of calculated and Arrhenius rate coefficients for $H_2O + N_2$ reaction.

The molecular dynamics cross-section data were used in the DSMC calculations to determine the probability of H_2O–N_2 dissociation as a function of the internal energy of water and the relative H_2O–N_2 collision speed.

IV. Numerical Technique and Collision Models

The SMILE computational tool based on the DSMC method was used in the computations. Details on the tool may be found elsewhere.[17] The SMILE capabilities that were used in the present work include models for energy transfer, two-level rectangular grids adaptive to flow gradients, different grids for collisions and macroparameters, and parallel implementation with efficient load balancing techniques. The numerical parameters used were similar to those used by Levin et al.[5] The number of simulated molecules in the computational domain was approximately 1,300,000, a sufficient value to avoid the influence of statistical dependence on the modeling results. Separate grids were used for modeling collisions and macroparameters adaptive to flow gradients. The total number of collision and macroparameter cells was 150,000 and 30,000, respectively.

The majorant frequency scheme was employed for modeling molecular collisions.[18] The VHS model was used for modeling intermolecular interactions.[6] The discrete Larsen–Borgnakke model[11] (also see Refs. 19 and 20) with temperature-dependent and constant values for rotational[21] and vibrational[22] relaxation numbers was utilized for rotation–translation and vibration–translation energy transfer. Because correct modeling of H_2O internal energy states is important to predict OH production correctly, special attention was paid to the H_2O–N_2 relaxation rate. Constant values of 250 and 15 were used for vibrational and rotational collision numbers Z_v and Z_r, respectively.[23,24] The TCE model[7] was employed to calculate the cross sections for all gas-phase chemical reactions involving the chemical species N_2 and O_2 and their derivatives. The complete list of N_2–O_2 reactions may be found in earlier work,[25] and the additional OH-producing reactions used in this work are given in Table 2 (see Refs. 2, 8, and 26). The H_2O–N_2 dissociation cross sections were obtained from the MD calculations, as already discussed, and from the TCE model.

The OH and H_2O species were considered as trace species whose weighting factor was varied from 10^{-5} to 10^{-9} depending on the altitude of the simulation. The species weighting scheme[6,27] was utilized in the computations. Models used for energy redistribution were discussed in Sec. II.

Finally, gas–surface interactions were assumed to follow a Maxwell model. Three different accommodation coefficients were utilized for translational, rotational, and vibrational modes of reflected molecules. A value of 0.85 for the translational accommodation coefficient was assumed, whereas a smaller value of 0.5 was used for the internal energy accommodation coefficients.[5] For high-energy collisions simulated in this work, the internal energy accommodation coefficients may be even lower.[28]

V. Results and Discussion

The results in this section include a discussion of the general properties of the flowfield and a description of the resulting OH vibrational distributions and number densities. The contribution of different OH production mechanisms are compared at two altitudes, and the reasons for the difference in results obtained using different dissociation models are explored.

A. General Flowfield Features

The computations were performed for a flow about a 0.2-m-diam sphere. The flow velocity is 5.1 km/s, and the freestream conditions

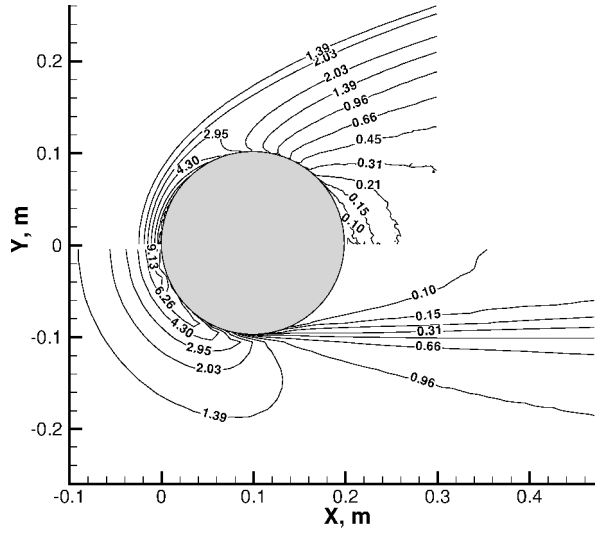

Fig. 4 Comparison of total number densities normalized by freestream values for 80 km (top) and 100 km (bottom).

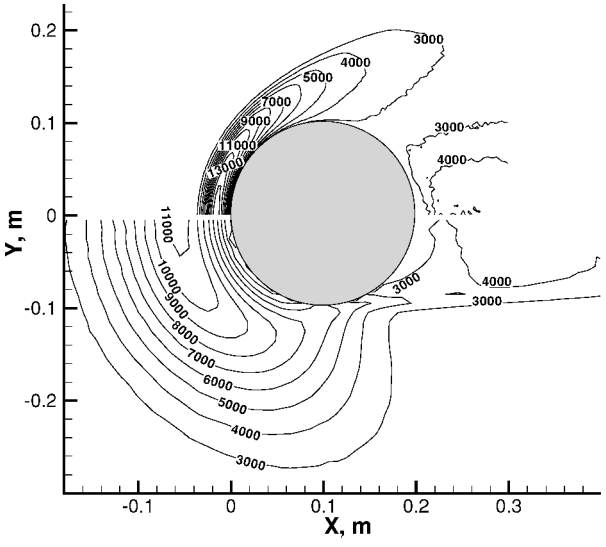

Fig. 5 Comparison of translational temperature (degrees Kelvin) for 80 km (top) and 100 km (bottom).

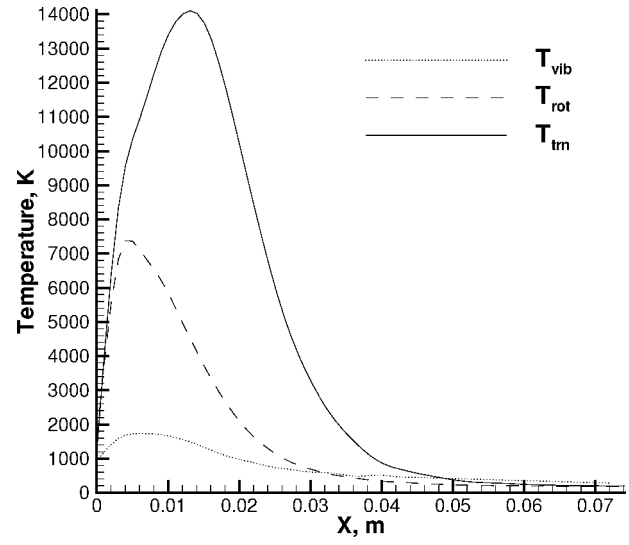

Fig. 6 N_2 temperature profiles along the stagnation streamline for 80 km.

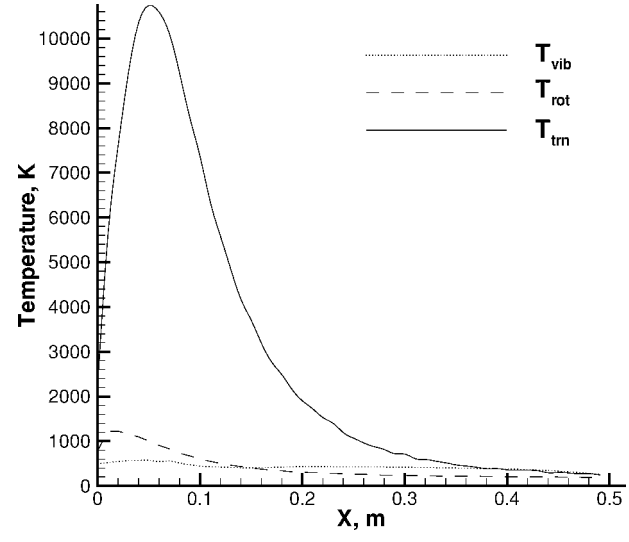

Fig. 7 N_2 temperature profiles along the stagnation streamline for 100 km.

are given in Table 1 for the two altitudes for which results will be shown. Note here that the properties of the major flow species N_2, O_2, and O are not sensitive to the OH production chemistry models. In this subsection, we discuss the macroscopic parameters of the flow.

Figure 4 shows the total number density contours for 80 and 100 km. Figure 4 illustrates the growth of the shock-layer width as the rarefaction increases. The shock wave is merged with the boundary layer for both cases because the flow rarefaction is high even for 80 km, where the Knudsen number is 0.03. Figure 5 shows the corresponding translational temperature contours for 80- and 100-km altitude. The maximum translational temperatures at both altitudes is approximately the same, with a somewhat higher value at 80 km. The translational temperature is an important property that determines the the rates of chemical processes. However, a significant degree of translational nonequilibrium, that is, non-Maxwellian two-peak velocity distribution functions, complicates the use of temperatures to calculate the production of trace species such as OH formed by chemical reactions.

The degree of nonequilibrium between translational and internal modes is also an important factor for chemical processes. The difference in the bulk translational, rotational, and vibrational temperatures for the two altitudes under consideration can be seen in closer detail by examining the spatial distribution along the stagnation streamline. Figures 6 and 7 show that the flow exhibits thermal nonequilibrium both at 100 and 80 km. (Here, X is the distance from the body surface.) The higher collision rate at 80 km causes all temperatures to be higher than the respective values at 100 km. At 100 km, the vibrational and rotational temperatures are too small to contribute significantly to the reaction cross sections, with the translational mode being the most important.

B. Contribution of OH Production Processes at 80 and 100 Kilometers

Figures 8 and 9 show the contributions of different OH production reactions at 80 and 100 km, respectively, using the TCE model. The calculations were performed for each reaction separately to isolate the relative contribution.

At 80 km, the most important reaction leading to OH production is water dissociation. The water exchange reaction, which leads to approximately the same OH number density at the body surface, starts later in the shock, because the rate of this reaction depends on the O concentration. At 80 km, there is almost no O in the freestream, so that the reaction starts only after enough O is produced in the shock by oxygen dissociation. The contribution of the $H_2 + O$ reaction is more than an order of magnitude less than the contribution of reactions (1) and (2). Similar to Eq. (2), this reaction [Eq. (4)] starts to contribute at about the same point in the flow. The $H + O_2$ reaction

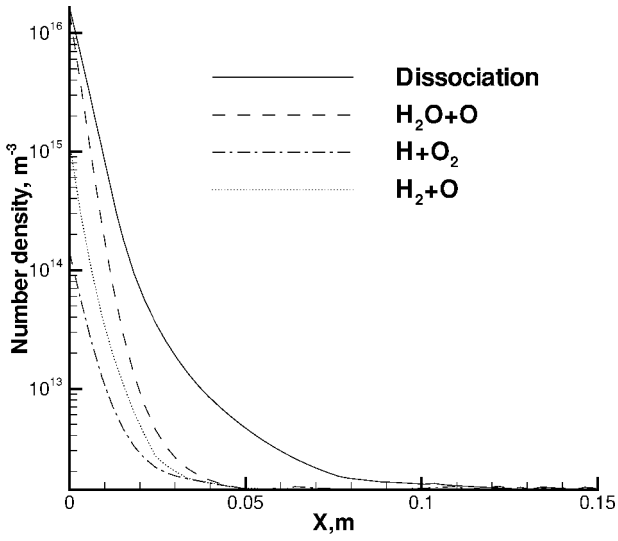

Fig. 8 OH number density profiles along the stagnation streamline at 80 km; contribution of different processes.

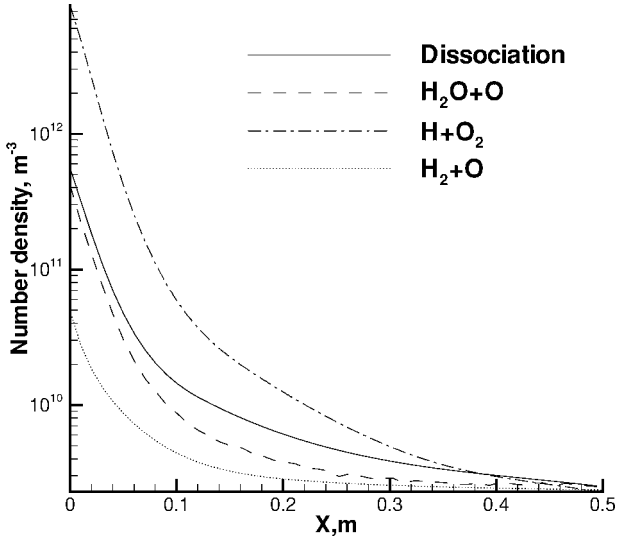

Fig. 9 OH number density profiles along the stagnation streamline at 100 km; contribution of different processes.

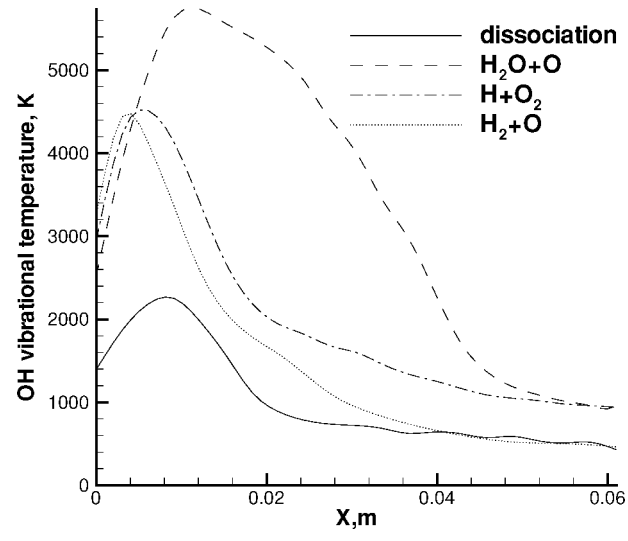

Fig. 10 OH vibrational temperature profiles along the stagnation streamline at 80 km.

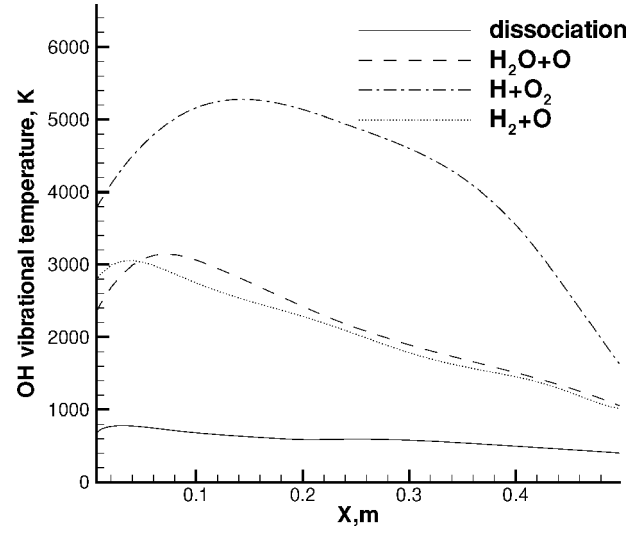

Fig. 11 OH vibrational temperature profiles along the stagnation streamline at 100 km.

has almost no impact on the overall OH production because of low freestream H concentration.

At 100 km, the order of importance changes, with the most important reaction becoming $H + O_2$ exchange [Eq. (3)]. At the body surface, the number density of OH produced by this reaction is about an order of magnitude larger than the number density of OH, produced by water dissociation [Eq. (1)]. As at 80 km, the contributions of water dissociation and water exchange are close, but there is no pronounced delay in the exchange reaction contribution because there is enough atomic oxygen in the freestream. The contribution of the $H_2 + O$ reaction is about an order of magnitude less than the contributions from water dissociation and exchange.

Although the relationship between water exchange and dissociation reactions and the $H_2 + O$ reaction is approximately the same at the two altitudes, the relative contribution of the $H + O_2$ reaction dramatically changes. This can be attributed to an abrupt change in the H mole fraction, from 5×10^{-8} at 80 km to 5×10^{-6} at 100 km.

Figure 10 shows profiles of the vibrational temperature of OH produced by the four processes at 80 km. Water dissociation, which was just shown to produce the most OH at this altitude, gives the lowest OH vibrational temperature. The maximum vibrational temperature of OH produced by dissociation is observed at about 1 cm from the wall, with the magnitude of slightly more than 2000 K. The reason for such low temperatures compared to the other reactions is the considerably higher reaction heat subtracted from the translational and internal energies of the reaction products. At 80 km, the highest OH vibrational temperature is produced by the $H_2O + O$ exchange reaction. This is mainly due to the process of energy equipartition over the reaction products used in the Larsen–Borgnakke[11] model. In water, there are three rotational and up to six vibrational modes that are noticeably excited (under the flow conditions at 80 km) leading to a significant amount of internal water energy that is distributed over OH internal modes.

The OH vibrational temperatures for the different reactions at 100 km are given in Fig. 11. All of the reactions give lower OH vibrational temperatures as compared to 80 km due to the lower internal temperatures of the reactants at 100 km. Comparison of Figs. 10 and 11 shows that dissociation reaction predicts much lower OH vibrational temperature at 100 km. The difference in vibrational temperatures at the two freestream conditions is due to the energy redistribution model used for the dissociation reaction. As already noted, in the Haas model[10] the OH internal energy is proportional to the H_2O internal energy. The important conclusion is that at 100 km the reaction $H + O_2$ gives the maximum OH vibrational temperature of over 5000 K. Because this reaction produces the maximum number density compared to the three other processes, it could be an explanation for the high OH vibrational temperature observed in the experimental spectra.[1]

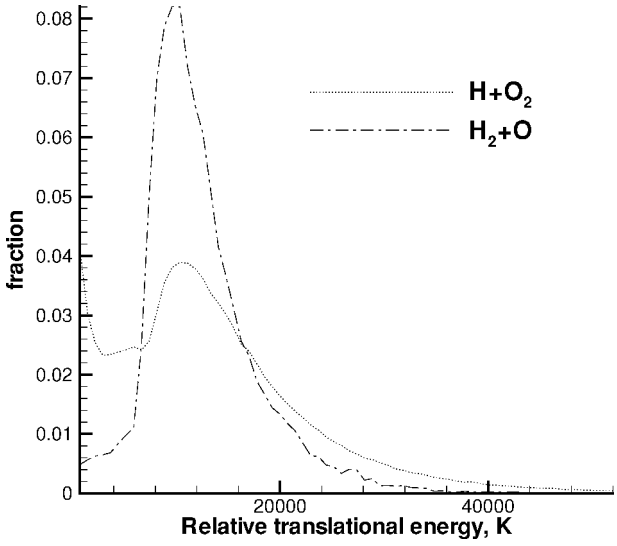

Fig. 12 Relative translational energy distribution of reactants at 100 km.

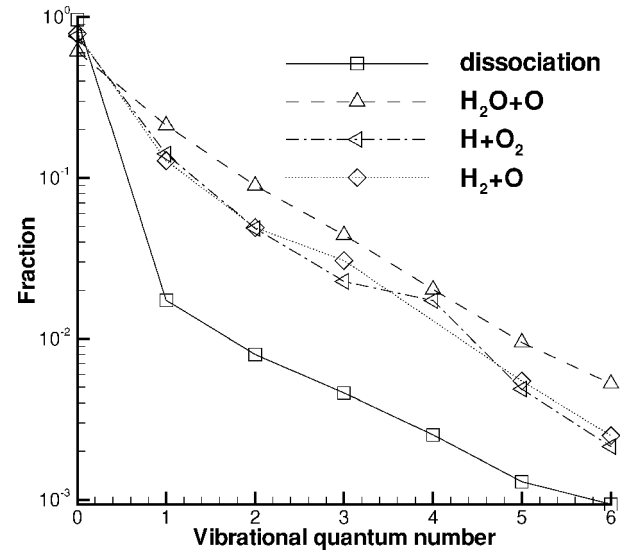

Fig. 13 OH vibrational distribution at 80 km shown at the point of maximum vibrational temperature.

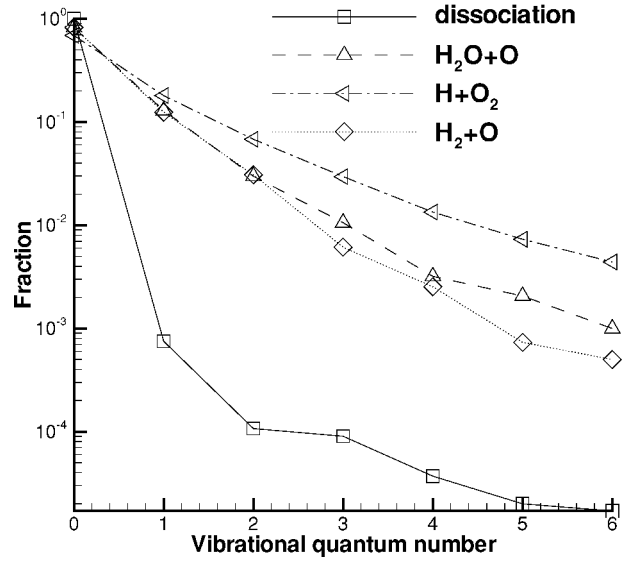

Fig. 14 OH vibrational distribution at 100 km shown at the point of maximum vibrational temperature.

The principal difference of the flow at 100 km as compared to that at 80 km is that the internal modes of all molecules in the flow are essentially unexcited. The relative translational energy is, therefore, the main contribution to the reaction energy. Under such conditions, reactions (3) and (4) were expected to give similar OH vibrational temperatures. However, examination of the OH vibrational temperature profiles at 100 km shown in Fig. 11 does not support that conclusion.

Figure 12 gives a possible explanation for the large difference in OH vibrational temperature for reactions (3) and (4). The distribution function of the relative collision velocity of the reactants for the two processes summed over all reactions in the computational domain is presented in Fig. 12. It is seen that the high-energy tail is significantly higher for the $H + O_2$ reaction, which causes more OH molecules to be formed in higher vibrational states. The wider distribution function for the $H + O_2$ collisions in the shock front is due to the smaller reduced mass of the colliders in Eq. (3) as compared to Eq. (4).

As was mentioned in the Introduction, the most important characteristic that determines the ratio between the spectral maxima at 2800 and 3100 Å is the ratio of the OH(A) vibrational populations in the first and zeroth vibrational states. The population of the OH(A) vibrational levels is assumed to be the same as that of OH. Because the OH vibrational populations may be non-Boltzmann in the shock front, an assessment of that ratio based on vibrational temperature would be inaccurate.

The normalized populations of vibrational levels 0–6 are shown in Figs. 13 and 14 for the different reactions at altitudes of 80 and 100 km, respectively. At 80 km, the vibrational populations are nonequilibrium for all reactions except for the $H_2O + O$ exchange. At 100 km, all of the vibrational distributions are nonequilibrium. The distributions may be approximated by two temperatures, one based on the first two vibrational levels and the other based on vibrational levels one and higher.

The observed nonequilibrium is a result of the combined influence of several factors. First, the distributions of velocities and energies of reactants are strongly nonequilibrium, which results in some degree of nonequilibrium in the reaction products. Then, the subtraction of a large reaction heat in the dissociation reaction along with the proportional energy redistribution of the Haas model[10] can also promote vibrational nonequilibrium of OH. Also, there is some number of vibrationally cold OH molecules from the freestream. If chemical reactions produce only a small number of OH molecules, the relative importance of these freestream OH molecules increases. Finally, half of the molecules reflected from the wall will have full internal energy accommodation. Most of the reflected molecules will be in the ground vibrational state, and some of them will penetrate upstream to the point of the highest vibrational temperature.

VI. Impact of the Dissociation Reaction Model on the OH Production

The total collision energy model[7] for chemical reactions was used in the computations presented in the preceding sections. Whereas the model has been used in DSMC calculations for over two decades and is conventionally regarded as a standard DSMC chemistry model, the accuracy of the model in highly nonequilibrium conditions is questionable. One of the most commonly used alternatives to the TCE model for modeling the dissociation process with the DSMC method is an approach that incorporates, to some extent, vibration–dissociation coupling.[29] The general concept is that the contribution of the vibrational energy modes to the energy of reaction is more efficient than that of the other modes. That means that if two colliding pairs have same total energy (the sum of the relative translational and internal), the pair with the larger vibrational energy has a higher reaction probability. Whereas the dissociation reaction for diatomic molecules has been studied extensively using the DSMC method and different models have been suggested, the dissociation of polyatomics as well as the exchange reactions of diatomics have not been examined in detail.

To understand the sensitivity of the flow modeling to the chemistry model, we used several models for the water dissociation reaction

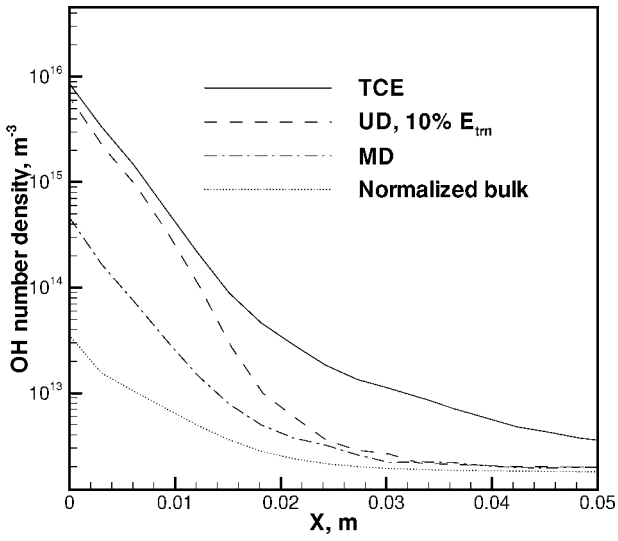

Fig. 15 OH number density profiles along the stagnation line at 80 km due to $H_2O + N_2$ dissociation reaction calculated using different dissociation models.

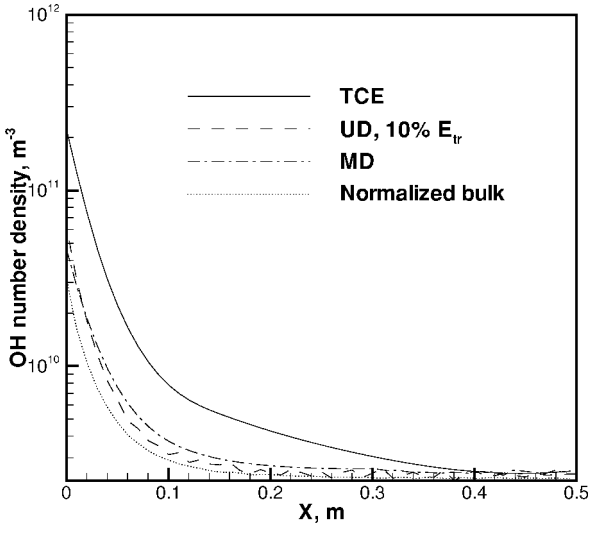

Fig. 16 OH number density profiles along the stagnation line at 100 km due to $H_2O + N_2$ dissociation reaction calculated using different dissociation models.

Eq. (1) in the DSMC flow modeling. In addition to the TCE model, we present the results for a model based on the trajectory computations for the $N_2 + H_2O$ dissociation process as well as the model[5] based on the unimolecular dissociation (UD) of water. In the UD model, the collision time was assumed to be the ratio of the VHS collision diameter to the relative velocity of the colliding pair, and the contribution of the relative translational energy to the reaction energy was taken to be 10% (Ref. 5).

The OH number density along the stagnation line at 80 km is shown in Fig. 15 for the different dissociation models. The bulk number density normalized by the OH freestream concentration is also given in Fig. 15 to illustrate the increase in the number density that can be attributed to the formation of a bow shock. Note that the normalized bulk number density values are lower than those for the dominant OH production mechanisms given in Figs. 8 and 9. Both the MD and UD models manifest a significant delay in the OH number density increase. This delay is due to the dissociation induction time necessary to excite water internal energy modes. The OH number density predicted by the UD model then approaches that obtained with the TCE model with a difference of less than 50% near the surface. Compared to the UD model, the MD model shows lower OH production, probably due to the higher degree of vibration–dissociation coupling.

OH number density along the stagnation line at 100 km, calculated using different dissociation models, is shown on Fig. 16. Here both the UD and MD models predict significantly lower OH number density than the TCE model. Moreover, because in both these models OH production strongly depends on the amount of internal energy of water and the internal energy modes are essentially unexcited at 100 km, the OH number density only slightly exceeds the normalized bulk density. The UD and MD models predict that almost no dissociation occurs at 100 km.

VII. Conclusions

The DSMC method was used to calculate the flowfields in the bow shock at 80 and 100 km. The main goal of this work was to elucidate the possible mechanism for the production of vibrationally hot OH(A) observed in the BSUV 2 experiment at 100 km. The TCE model was used to calculate reaction probabilities for all reactions. The reaction probabilities obtained by the MD/QCT method were used to provide more detailed modeling of the $H_2O + N_2$ dissociation reaction.

Four main processes that contribute to OH production in the flow were discussed: water dissociation, the exchange reaction between water and atomic oxygen, and the exchange reactions between hydrogen and oxygen. In general, the OH vibrational temperature at 100 km is significantly higher than at 80 km, because the contribution of different mechanisms of OH production changes as a function of altitude.

The calculations showed that at 100 km the main mechanism leading to OH production is the $H + O_2$ exchange reaction. This reaction also gives the highest vibrational temperature in the shock wave (more than 5000 K). The number density of OH produced by this reaction as well as high OH vibrational temperature suggest that this mechanism may explain the BSUV 2 spectral data at 100 km. However, future flight experiments that simultaneously measure radiation and freestream conditions (by mass spectroscopy) would provide a definitive spectral data set.

Water dissociation gives very low OH vibrational temperatures at 100-km altitude. At 80 km, the main mechanism of OH formation is the collisionally induced water dissociation. The dissociation mechanism gives higher OH vibrational temperatures than at 100 km, with a maximum OH vibrational temperature of about 2500 K.

As was shown earlier, MD gave a much lower OH dissociation rate compared to the TCE model because in this model the reaction probability strongly depends on the internal water energy. At 100 km, there is little excitation of water internal energy modes. The PES is approximate in that internal energy exchange between N_2 and water is neglected. However, comparison of the computed MD water dissociation rates with shock-tube data shows that the assumption of energy exchange in water dissociation is dominated by relative translational to water internal energy exchange. Hence, the MD probability of reactions used in the DSMC simulations present a more accurate assessment of water dissociation than the TCE model.

Acknowledgments

The work at George Washington University and Pennsylvania State University was supported by Army Research Office Grant DAAG55-98-1-009 for the Ballistic Missile Defense Organization and Air Force Office of Scientific Research Grant F49620-99-1-0143.

References

[1]Levin, D., Collins, R., Candler, G., Wright, M., and Erdman, P., "Examination of OH Ultraviolet Radiation from Shock-Heated Air," *Journal of Thermophysics and Heat Transfer*, Vol. 10, No. 2, 1996, pp. 200–208.

[2]Baulch, D. L., Drysdale, D. D., Home, D. G., and Lloyd, A. C., "Evaluated Kinetic Data for High Temperature Reactions," *Homogeneous Gas Phase Reactions of the H_2–O_2 System*, Vol. 1, Butterworths, London, 1972.

[3]Levin, D., Laux, C., and Kruger, C., "A General Model for the Spectral Calculation of OH Radiation in the Ultraviolet," *Journal of Quantitative Spectroscopy and Radiative Transport*, Vol. 61, No. 3, 1999, pp. 377–392.

[4]Kossi, K. K., and Boyd, I. D., "Detailed Computation of Ultraviolet Spectra in Rarefied Hypersonic Flow," *Journal of Spacecraft and Rockets*, Vol. 35, No. 5, 1998, pp. 653–659.

[5]Levin, D. A., Gimelshein, N. E., and Gimelshein, S. F., "Examination of Water Dissociation Models in Shock-Heated Air," *Journal of Thermophysics and Heat Transfer*, Vol. 16, No. 2, 2002, pp. 251–260.

[6]Bird, G. A., *Molecular Gas Dynamics and the Direct Simulation of Gas Flows*, Clarendon, Oxford, 1994.

[7]Bird, G. A., "Monte-Carlo Simulation in an Engineering Context," *Rarefied Gas Dynamics*, edited by S. Fisher, Vol. 74, Progress in Astronautics and Aeronautics, AIAA, New York, 1981, pp. 239–255.

[8]Yang, H., Gardiner, W. C., Shin, K. S., and Fujii, N., "Shock Tube Study of the Rate Coefficient of $H + O_2$ to $OH + O$," *Chemical Physics Letters*, Vol. 231, No. 4–6, 1994, pp. 449–453.

[9]Brasseur, G., and Solomon, S., *Aeronomy of the Middle Atmosphere*, D. Reidel, Boston, 1986, Chap. 4.

[10]Haas, B. L.,"Modeling of Energy-Exchange Mechanics Applicable to a Particle Simulation of Reactive Flows," *Journal of Thermophysics and Heat Transfer*, Vol. 6, No. 2, 1992, pp. 200–207.

[11]Borgnakke, C., and Larsen, P. S., "Statistical Collision Model for Monte Carlo Simulation of Polyatomic Gas Mixture," *Journal of Computational Physics*, Vol. 18, No. 4, 1975, pp. 405–420.

[12]Murrell, J. H., Carter, S., Farantos, S. C., Huxley, P., and Varandas, A. J. C., *Molecular Potential Energy Functions*, Wiley, New York, 1984, Chap. 5.

[13]Redmon, M. J., Schatz, G. C., and Garrett, B. C., "Theoretical Studies of Vibrational Excitation in Collisions of $O(^3P)$ with $H_2O(^1A_1)$," *Journal of Chemical Physics*, Vol. 84, No. 2, 1984, pp. 764–773.

[14]Schmidt, M. W., Baldridge, K. K., Boatz, J. A., Elbert, S. T., Gordon, M. S., Jensen, J. H., Koseki, S., Matsunaga, N., Nguyen, K. A., Su, S., Windus, T. L., Dupuis, M., and Montgomery, J. A., Jr., "The General Atomic and Molecular Electronic Structure System," *Journal of Computational Chemistry*, Vol. 14, 1993, p. 1347.

[15]Nyman, G., Rynefors, K., and Holmlid, L., "Efficient Microcanonical Sampling for Triatomic Molecular Systems: Exact Distributions Verified," *Journal of Chemical Physics*, Vol. 88, No. 6, 1986, pp. 3571–3580.

[16]Herzberg, G., *Molecular Spectra and Molecular Structure*, D. Van Nostrand, Princeton, NJ, 1960, Chap. 3.

[17]Ivanov, M. S., Markelov, G. N., and Gimelshein, S. F., "Statistical Simulation of Reactive Rarefied Flows: Numerical Approach and Applications," AIAA Paper 98-2669, June 1998.

[18]Ivanov, M. S., and Rogasinsky, S. V., "Theoretical Analysis of Traditional and Modern Schemes of the DSMC Method," *Proceedings of the XVIIth International Symposium on Rarefied Gas Dynamics*, edited by A. E. Beylich, VCH Verlagsgesellschaft, Weinheim, Germany, 1990, pp. 629–642.

[19]Boyd, I. D., "Relaxation of Discrete Rotational Energy Distributions Using a Monte Carlo Method," *Physics of Fluids A*, Vol. 5, No. 9, 1993, pp. 2278–2286.

[20]Gimelshein, S. F., Boyd, I. D., and Ivanov, M. S., "Modeling of Internal Energy Transfer in Plume Flows of Polyatomic Molecules by the DSMC Method," AIAA Paper 99-0738, Jan. 1999.

[21]Parker, J. G., "Rotational and Vibrational Relaxation in Diatomic Gases," *Physics of Fluids*, Vol. 2, No. 4, 1959, pp. 449–462.

[22]Millikan, R. C., and White, D. R., "Systematics of Vibrational Relaxation," *Journal of Chemical Physics*, Vol. 39, No. 12, 1966, pp. 3209–3213.

[23]Dunn, M. G., Skinner, G. T., and Treanor, C. E., "Infrared Radiation from H_2O, CO_2, or NH_3 Collisionally Exited by N_2, O, or Ar," *AIAA Journal*, Vol. 13, No. 6, 1973, pp. 803–812.

[24]Kung, R. T. V., and Center, R. E., "High Temperature Vibrational Relaxation of H_2O by H_2O, He, Ar and N_2," *Journal of Chemical Physics*, Vol. 62, No. 6, 1975, pp. 2187–2194.

[25]Gimelshein, S. F., Levin, D. A., and Collins, R. J., "Modeling of Spacecraft Glow Radiation in Flows About a Reentry Vehicle at High Altitudes," *Journal of Thermophysics and Heat Transfer*, Vol. 14, No. 4, 2000, pp. 471–479.

[26]Hwang, R. S., and Rabinowitz, M. J., "Rate Coefficient of the $O + H_2 \rightarrow OH + H$ Reaction Determined via Shock-Tube Laser Absorption Spectroscopy," *Chemical Physics Letters*, Vol. 242, No. 3, 1995, pp. 279–284.

[27]Gimelshein, S. F., Levin, D. A., and Collins, R. J., "Modeling of Infrared Radiation in a Space Transportation System Environment," *AIAA Journal*, Vol. 40, No. 4, 2002, pp. 781–790.

[28]Boyd, I., Phillips, W., and Levin, D., "Prediction of Ultraviolet Radiation in Nonequilibrium Hypersonic Bow-Shock Waves," *Journal of Thermophysics and Heat Transfer*, Vol. 12, No. 1, 1998, pp. 38–44.

[29]Haas, B. L., and Boyd, I. D., "Models for Direct Monte Carlo Simulation of Coupled Vibration-Dissociation," *Physics of Fluids A*, Vol. 5, No. 2, 1993, pp. 478–489.

G. V. Candler
Associate Editor